THE JOURNAL OF PHYSICAL CHEMISTRY C

Article

pubs.acs.org/JPCC

Angular Redistribution of Near-Infrared Emission from Quantum Dots in Three-Dimensional Photonic Crystals

Bart H. Husken,*[,†,‡] A. Femius Koenderink,[‡] and Willem L. Vos[†]

[†]Complex Photonic Systems (COPS), MESA[+] Institute for Nanotechnology and Department of Science and Technology, University of Twente, P.O. Box 217, 7500 AE Enschede, The Netherlands

[‡]Center for Nanophotonics, FOM Institute AMOLF, Science Park 104, 1098 XG Amsterdam, The Netherlands

ABSTRACT: We study the angle-resolved spontaneous emission of near-infrared light sources in three-dimensional photonic crystals over a wavelength range 1200−1550 nm. To this end, PbSe quantum dots are used as light sources inside titania inverse opal photonic crystals. Strong deviations from the Lambertian emission profile are observed. An attenuation of 60% is observed in the angle-dependent radiant flux emitted due to photonic stop bands. At angles that correspond to the edges of the stop band, the emitted flux is increased by up to 34%. This increase is explained by the redistribution of Bragg-diffracted light over the available escape angles. The results are quantitatively explained by an expanded escape-function model. This model is based on diffusion theory and adapted to photonic crystals using band structure calculations. We identify the need to separately consider the transport mean free path of both the emitted light and the light used for excitation. Here, the model is applied to describe emission in the regime where samples are optically thick for the excitation light, yet relatively thin for the photoluminescence light.

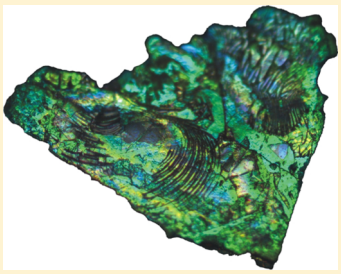

INTRODUCTION

There is much interest in nanophotonic control over the spontaneous emission of light.[1−3] Therefore, emission properties of light sources such as atoms, molecules, and quantum dots embedded in a myriad of nanostructures are studied intensively. The spontaneous emission rate of these light sources is described by Fermi's golden rule. The golden rule shows that the spontaneous emission rate is proportional to a local property called the local density of optical states (LDOS).[4] Indeed, recent experiments have demonstrated that it is possible to control the LDOS and thereby the spontaneous emission rate, for example, using photonic crystals.[5−13]

A second important aspect of photonic crystals is their ability to strongly influence the directional emission spectrum from embedded light sources, such that the emission deviates strongly from Lambertian emitters. These spectral changes are stop bands caused by stop gaps in the photonic bandstructures as a result of optical Bragg diffraction.[14−25] In addition to gap formation, ubiquitous deviations from the perfect crystal give rise to multiple scattering and diffusion of light.[26−35] Although there are many qualitative studies on light transport in photonic crystals, there exist only a few quantitative papers. One of the central concerns regarding light emission from photonic crystals is the angular distribution, or *escape function*, of the emitted light over exit angles. Fundamental insight in this escape probability distribution is needed to explain the photonic crystal properties and the crystals' influence on the radiative emission of the light source. Surprisingly, the escape function is often disregarded, which may easily lead to misinterpretations of experimental results. Hence, detailed knowledge about the escape function and a comparison to the emission spectra from nonphotonic reference crystals are essential to find the cause of changes in the measured emission spectrum.

Most experimental work on light emission in photonic crystals and the corresponding escape function is limited to the visible range. For experiments on very strongly interacting photonic crystals made of semiconductors such as silicon,[36−38] near-infrared emitting light sources are important, in particular versatile quantum dots such as PbSe and PbS (λ > 1100 nm).[39−42] The ability to control spontaneous emission and light propagation at these frequencies is of keen interest for applications, as spontaneous emission is a limiting factor in numerous devices.[1,43,44] Emission control therefore implies a substantial increase in efficiency in applications such as light beaming, reflector design, and light harvesting.[45−47] Furthermore, guiding of light can be used to enhance the collection efficiency in single photon on demand applications. In this paper, emitted light escaping from three-dimensional (3D) photonic crystals is studied at near-infrared wavelengths in the range 1200−1550 nm. To this end, colloidal PbSe quantum dots are used as light sources inside strongly photonic titania inverse opal photonic crystals with a range of lattice parameters.

EXPERIMENTAL DETAILS

The samples consist of commercially available PbSe quantum dots[39−42,45,48−50] (Evident Technologies) embedded inside titania inverse opal photonic crystals. See refs 51 and 52 for a detailed description of the fabrication and characterization of these crystals that are made by template-assisted assembly. X-

Received: August 29, 2012
Revised: December 12, 2012
Published: December 13, 2012

ray diffraction and scanning electron microscopy studies show that the crystals have face centered cubic (fcc) crystal structure and that the direction perpendicular to the samples' surface corresponds to the (111) direction.[52] The small-angle X-ray scattering experiments confirm an excellent long-range periodic ordering of our crystals. The inverse opals were made from opal templates with sphere radii r = 340−655 nm, in order to yield low order stop bands (corresponding to the L-gap in photonic band structures) in the emission spectrum of the quantum dots. Additionally, r < 200 nm spheres are used for reference measurements. For these radii, the lattice parameter a is on purpose so small that photonic stop bands are blueshifted relative to the quantum dot emission spectra. Therefore, these reference crystals are in the long-wavelength limit and are referred to as *nonphotonic*.[53]

Not all fabricated structures are suited for the emission experiments. Parts of the crystals were found to be covered with bulk titania or the air−sphere ordering may be poor. Visually, samples that show clear Bragg diffraction are selected for further study. Subsequently, bright-field microscope images are made to chart each sample, such that specific locations can be retrieved in different experimental setups.[54] Finally, reflectivity measurements are used to reveal the areas with clear stop bands that are suitable for subsequent emission experiments.

The useful samples are infiltrated with colloidal PbSe quantum dots using methods similar to refs 5, 7, 17, and 21. Each sample is placed in a 5 mL glass vial. Next, 50 μL of 0.92 μM PbSe quantum dots in hexane suspension is added. After one day, the suspension is removed, and the samples are rinsed three times with hexane, each time for 20 s. Subsequently, the sample is dried in a nitrogen-purged chamber for one day. The infiltration leads to a random distribution of quantum dots on the titania−air surfaces inside the inverse opals. From the concentration of dots in the suspension and the volume of the air spheres with typical radii of 385 nm, the distance between adjacent quantum dots is estimated to be 120 nm. This is sufficiently large to avoid reabsorption and energy-transfer processes between the bulk of the dots.[55] In the Results section below, it is deduced that the quantum dots are truly inside the photonic crystal.

To prevent photo-oxidation of the quantum dots, the sample preparation and handling was carried out in a high-quality nitrogen-purged glovebox (MBraun, LabStar). For optical measurements, the samples were glued to the side of a needle pin, mounted in a sealed chamber, and kept under a 1.6 bar nitrogen atmosphere. Figure 1a shows the home-built chamber that is mounted on a rotation stage via a threaded ring at the bottom. Between this ring and the chamber, stages are visible that are used to tilt and translate the chamber. Figure 1b shows how a sample is glued to a needle pin. As only the thin side of the crystal is in contact with the needle, both the frontside and backside of the sample are accessible for the optical experiments discussed below.

Figure 2 shows the basic concept of the experiment. The sample is illuminated by a slightly focused laser beam of wavelength λ = 532 nm. The excitation spot radius is estimated to be about 7 μm. Light emitted from the sample is collected by a 0.05 NA objective and sent to a spectrometer (PI/Acton sp2558 spetrograph with OMA-V 1024/LN diode array). An 850 nm long-pass filter blocks the laser light in the detection path. The angle Θ_E is defined as the angle between the direction normal to the sample surface and the direction wherein the emission is collected. Θ_P refers to the angle

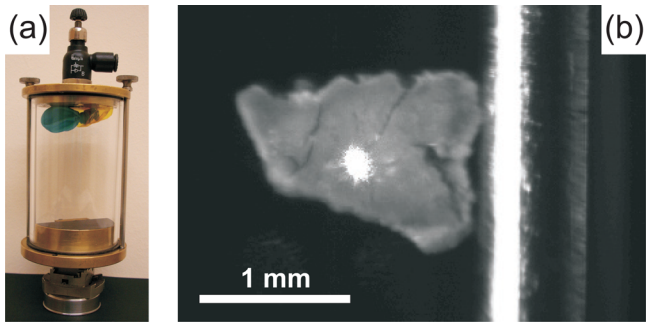

Figure 1. (a) Photograph of the sealed chamber used in the optical experiments. A transparent cylinder is sealed by two plates. The bottom plate is mounted on four stages that are fixed to a rotation stage. The top plate contains a valve to purge the chamber with nitrogen. (b) Front-view, gray scale image of a titania inverse opal photonic crystal glued to a needle pin (on the right). The white spot on the sample is a λ = 532 nm laser spot that is used to locally excite PbSe quantum dots inside this structure. Due to a combination of diffusion, scattering, and camera exposure time, the size of the laser spot appears much larger than the size of the actual focus (radius ≈ 7 μm).

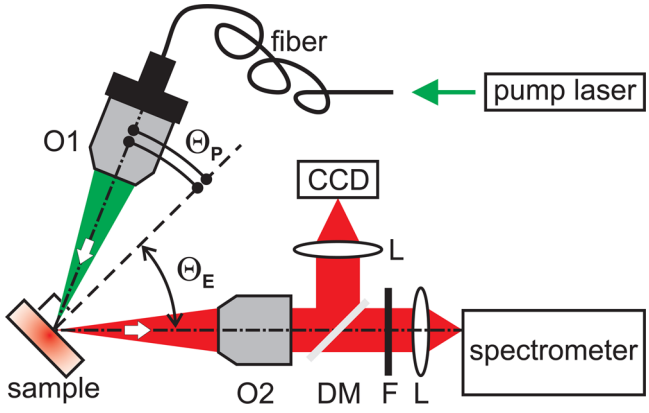

Figure 2. Schematic representation of the experiment. Light from a λ = 532 nm pump laser is coupled into a single mode fiber and used to excite quantum dots in a sample through objective O1. Near-infrared emission from the dots is collected with objective O2 and sent to a spectrometer. A long-pass filter (F) blocks the laser light. An achromat lens (L) focuses the collected light onto the entrance slit of the spectrometer. A dichroic mirror (DM) is used to guide the visible light to a camera for alignment purposes. The sample is rotated together with the pump beam such that angle Θ_P is fixed and the emission collection angle Θ_E changes. Consequently, the excitation conditions are the same for every angle Θ_P. The white arrows indicate the propagation direction of the light.

between the surface normal and the direction of the excitation beam. The sample and excitation objective are rotated together, such that Θ_P remains fixed while the collection angle Θ_E is varied, as in ref 21. After changing this detection angle, a CCD camera is used to roughly reposition the sample such that the illuminated spot is in focus with the spectrometer. Subsequent XYZ fine-tuning of the sample alignment was done by optimization to the emission signal measured with the spectrometer. The sample surface projected onto the entrance slit of the spectrometer changes with Θ_E. The measured intensities are corrected for this effect (in this paper we adopt the commonly used term *intensity* for what is actually the radiant flux), as discussed in ref 21. The current configuration

dx.doi.org/10.1021/jp308590g | J. Phys. Chem. C 2013, 117, 3431−3439

allows the emission detection over an unrivalled range of both positive and negative angles.

Emission from the titania backbone was experimentally found to be negligible at the near-infrared emission wavelengths of our quantum dots (1200−1500 nm), whereas backbone emission was noticeable in earlier experiments in the visible range.[7] Reasonably, the titania emission is expected from defect luminescence in the middle of the titania band gap, that is, in the visible range, and in the near infrared.

To reduce systematic errors, the emission detection angle Θ_E is varied in the following way. First, Θ_E is increased from 0° to maximum positive angles in steps of 20°. Subsequently, the angle is decreased in steps of 20° to maximum negative angles, which results in a data set with steps $\Delta\Theta_E = 10°$. For some measurements, the procedure is repeated to obtain a data set with steps $\Delta\Theta_E = 5°$. The experiment ends where it started, at $\Theta_E = 0°$. At the start and at the end of the experiment, the excitation laser is blocked after which the background signal is determined. As a result, the reproducibility of the measurement can be judged for all frequencies and in all experiments. For the typical integration times of 30−100 s, error bars of 1% of the measured number of counts per wavelength bin can be used to estimate the uncertainty in the measurement. When the emission spectrum of the dots changes with time, sawtoothlike shapes appear in emission intensity versus Θ_E plots. Therefore, our measurement sequence allows the time-varying effects in the results to be evaluated after a measurement.

RESULTS

Angle-Resolved Emission. Reflectivity measurements on four samples with different lattice parameters are shown in Figure 3 (reflectivity was measured with a separate setup as described in refs 31 and 56). Only measurements that show clear Bragg diffraction peaks are shown. The reflectivity is limited due to unavoidable structural disorder,[30] notably mosaic spread.[57] The emission spectrum of PbSe quantum dots is included in the same graph. The stop bands are overlapping or to the red of the quantum dot emission spectrum and far to the blue of the emission spectrum for reference measurements. Therefore, the fabricated samples cover the desired frequency (wavenumber ω) range from below to above the L-gap that is centered at frequency ω_{111}. The quality of the selected samples is comparable to samples used in earlier experiments in the visible range.[5,7,21] The areas that show the most powerful Bragg diffraction are used in subsequent emission experiments.

To verify that the quantum dots are truly inside the photonic crystal, a reference crystal was tested. Figure 4a shows the result

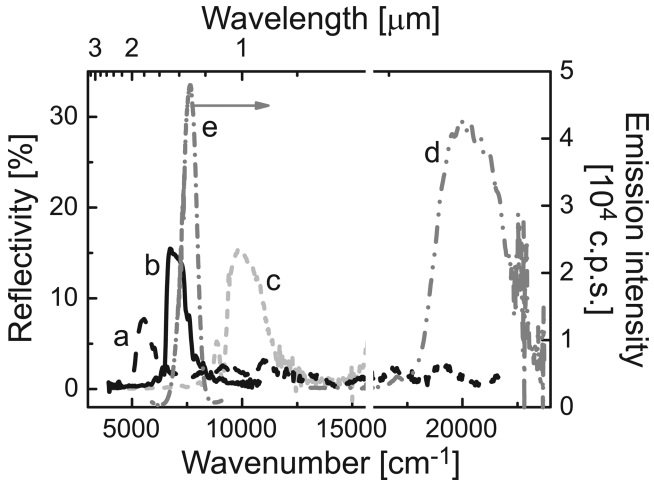

Figure 3. Normal-incidence reflectivity spectra measured from four titania inverse opals. These samples were grown from templates with different sphere radii r_{sphere}, namely, (a) 655 nm, (b) 515 nm, (c) 403 nm, and (d) 180 nm (left ordinate). Stop bands due to the L-gap appear as peaks in the reflectivity spectrum. (e) Shows the emission spectrum of PbSe quantum dots in a hexane suspension (right ordinate). The reflectivity is not defined in a narrow band around 15 800 cm^{-1} because of interference by a reference laser beam inside the spectrometer.

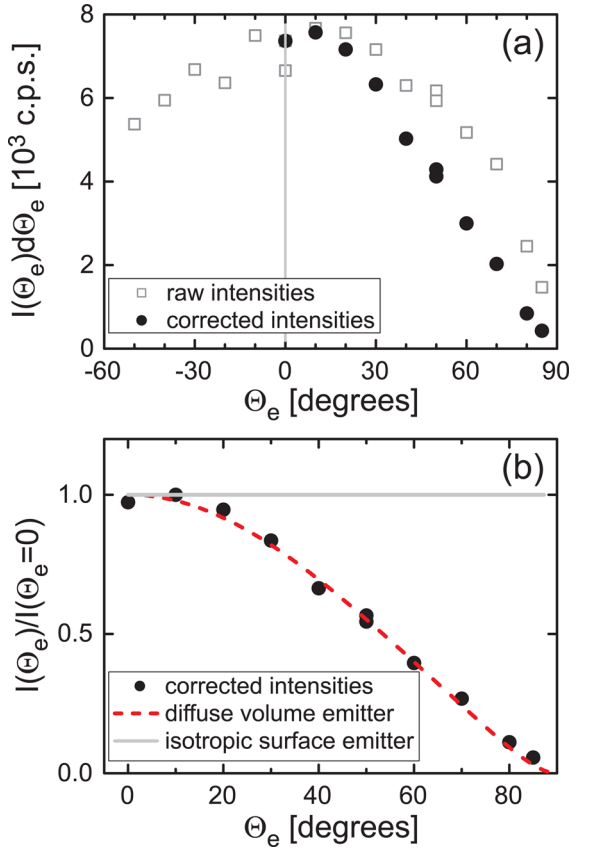

Figure 4. Angle-resolved emission intensity of PbSe quantum dots in a nonphotonic titania inverse opal. The sample's measured stop band is centered around ω_{111} = 11 730 cm^{-1}, and the measurement is done at frequency ω = 7143 cm^{-1} (1400 nm). (a) Open squares are the measured, background subtracted, intensities. Filled dots show the measured data corrected for the detected area. The intensity tends to zero as the angle approaches $\Theta_e = 90°$. (b) Normalized emission intensity versus detection angle. Filled dots are the same as in (a). The dashed line is the model for a diffuse volume (i.e., Lambertian) emitter. Solid line shows the expected behavior for an isotropic surface emitter. Clearly, our measurements agree with the diffusion model.

of the angle-resolved emission experiment. The background subtracted data are shown as open squares. The intensity profile is the same for positive and negative angles, which confirms that we are mostly sampling reciprocal space in the directions of the L high-symmetry point (at 0°) to the U- or K-points at positive or negative angles. The symmetry furthermore indicates that the orientation dependence of the emission is completely decoupled from the geometry of the excitation beam. The black dots are the intensities corrected for the angle-dependent collection efficiency. The corrected data decrease with angle

dx.doi.org/10.1021/jp308590g | J. Phys. Chem. C 2013, 117, 3431−3439

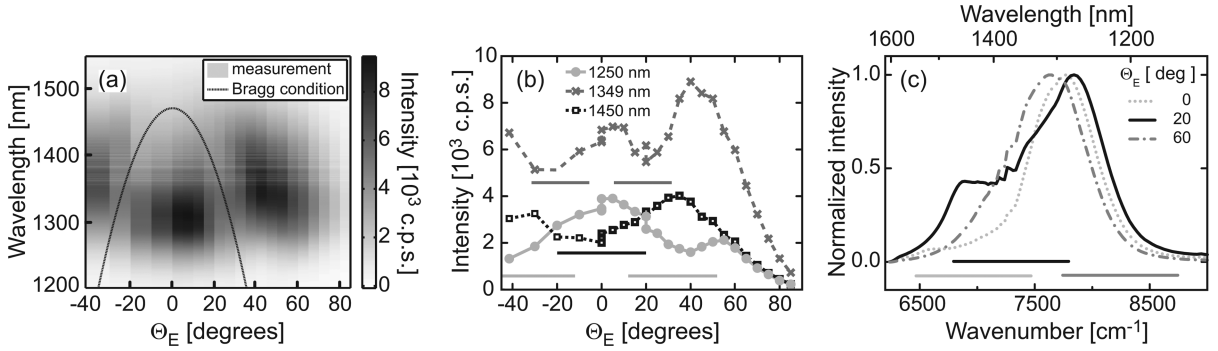

Figure 5. Measured PbSe quantum dot emission spectra from a photonic titania inverse opal with a measured stop band near wavenumber ω_{111} = 7000 cm^{-1}, background subtracted and detector surface area corrected. (a) Emission intensity as a function of wavelength and measured angle Θ_E. A clear suppression of emission intensity is observed in agreement with the Bragg condition (black curve). The white areas at wavelengths λ = 1200 and 1550 nm mark the boundaries of the quantum dot emission spectrum. (b) Cross sections of (a) at specific wavelengths show clear angular-dependent stop bands. (c) Cross sections of (a) at specific angles. The measured emission spectra are frequency dependent due to Bragg attenuation of the light in the stop band of the crystal and diffuse scattering. In (b,c) stop bands are indicated by the horizontal lines below the curves.

and tend to zero at 90° in agreement with Lambertian behavior, as expected for emitted light that is diffused in the bulk of a sample.

In Figure 4b, the corrected data from Figure 4a are normalized to their maximum at 0°. We compare the intensities to two models: (1) a model for emitters whose light has become diffuse in a bulk sample volume (discussed in detail in the Escape-Function Model section); and (2) a model where emitters are assumed to be limited to the surface of a sample. The latter model predicts a constant and angle-independent radiant flux that clearly disagrees with our data; hence, we can exclude that we probe only quantum dots on the surface of the sample. On the other hand, our data agree very well with the model for emitted light diffusing in a bulk volume. From this excellent correspondence, we conclude that we are indeed probing the emission of quantum dots that are located in the bulk of our samples.

Naively, one may conclude from the agreement between our measurements and the diffuse volume emitter model that the emitted light is diffuse, that is, multiply scattered in the bulk of the sample. From previous experiments on similar photonic crystals,[30,31] however, it is inferred that, at the long infrared wavelengths where our quantum dots emit ($\lambda \approx 1300$ nm), the ratio of sample thickness L to transport mean free path l of the light is as small as L/l = 3.1−9.5. (Our photonic crystals have lattice parameters a in the range 680−1310 nm, based on an assumed shrinkage of 30% between the template opal and final titania inverse opal.[52] The measured emission wavelength is in the range 1200−1550 nm. Hence, a/λ ranges 0.44−1.1, which corresponds to a l/a range from 100 (a = 680 nm) to 17 (a = 1310 nm).[30] Therefore, $l \approx 68$ μm and $l \approx 22$ μm for a = 680 nm and a = 1310 nm, respectively. With a sample thickness L = 210 μm,[52] L/l ranges from 3.1 to 9.5. Similarly, $L/l > 51$ for the excitation light at 532 nm.) References 30 and 31 studied light that is transmitted through the complete sample. In contrast, here, we study emission from light sources that are preferentially excited near the surface of incidence. Hence, the emitted light need not probe the complete sample thickness, and correspondingly, the calculated L/l values are even smaller in practice. Thus, the sample thickness is not much greater than the mean free path, and the emitted light is not very deeply in the diffusive regime. For these optical thicknesses, strong deviations from diffusion theory and radiative transport theory were reported.[58] This should be contrasted to the strongly diffusive regime $L/l > 10$ studied with emitters at shorter wavelengths in the visible range.[17,21] We surmise that the emission nonetheless appears diffuse for two additional reasons: the excitation light has such a short wavelength that the excitation is clearly in the diffuse regime. Moreover, the quantum dots inside the crystals have no preferred orientation of their transition dipole moments relative to the photonic crystal axes or the air−semiconductor interfaces inside the crystals. Therefore, the diffusion equation describes the spatial distribution of emission events in the bulk of the crystal well, and the emission has no preferred wave vector, in accordance with the wave vector content of multiply scattered light. As a consequence, it is reasonable that the angle-dependent intensities agree with a model for diffusion of emitted light in the bulk of the crystal.

Figure 5a shows extensive angle- and wavelength-dependent emission data measured on a photonic crystal in the range of the stop gaps. The emitted power is reduced in broad angular ranges, for example, between −20° and +20° at a wavelength of 1400 nm. Increase of the detection angle Θ_E results in a shift of the stop band toward shorter wavelengths. To a first approximation, this behavior can be explained by Braggs' law (black line). In Figure 5b,c, cross sections of (a) measured at constant wavelength or angle show the angular and wavelength dependence of the emitted power. The photonic crystal behaves very distinctly from a Lambertian emitter. The stop band causes a decrease of the measured emission intensity over an angular range of approximately 40°. In (c), the frequency of the emission intensity peak changes with angle. The peak is shifted to the blue if the stop band overlaps the red side of the spectrum, that is, at small angles. At larger angles, the stop band has moved to the blue part of the spectrum, and the emission peak is shifted somewhat to the red (not shown). At the largest angle, the peak shifts back to the frequency of the dots' actual emission maximum. This experiment demonstrates the influence of the photonic crystals' stop bands on the emission spectrum of the quantum dots: both attenuation and enhancements. The attenuation of a part of the emission spectrum resembles experimental observations using dye molecules[5,14−18,20−22,24] but was not previously observed with quantum dots.[21] An expanded escape-function model is used to quantitatively interpret the measurement. This is the topic of the next section.

dx.doi.org/10.1021/jp308590g | J. Phys. Chem. C 2013, 117, 3431−3439

Escape-Function Model. The model used to interpret the measured emission intensities is based on diffuse light transmission through multiple scattering, opaque media.[59−64] The model is expanded to photonic crystals following refs 21, 31, and 65. The approach consists of taking Bragg diffraction into account through the boundary conditions. Here, the most important relations are summarized to explain the essence of this model. Consider light emission in a sample. The emitted intensity $I(\omega; \mu_e)$ that escapes the sample at external angles between $\Theta_E = \cos^{-1}(\mu_e)$ and $\cos^{-1}(\mu_e + d\mu_e)$ with respect to the surface normal of the sample is written as

$$I(\omega; \mu_e)d\mu_e = I_{tot}(\omega)P(\omega; \mu_e)d\mu_e \quad (1)$$

Here, $I_{tot}(\omega)$ is the total spontaneously emitted intensity at frequency ω that exits the sample through the detection face. For sources with a low quantum efficiency or with inhomogeneously broadened spectra, $I_{tot}(\omega)$ is proportional to the LDOS.[5] $P(\omega; \mu_e)$ is a normalized probability distribution function that describes the distribution of photons over the available escape angles. We call $P(\omega; \mu_e)$ the *escape function* and use it to compare the model to experimental data. To determine $P(\omega; \mu_e)$ experimentally, eq 1 is rewritten such that

$$P(\omega; \mu_e) = \frac{I(\omega; \mu_e)}{I_{tot}(\omega)} \quad (2)$$

The numerator is given by the measured intensity, and the denominator $I_{tot}(\omega)$ is determined by summing the measured $I(\omega; \mu_e)$ weighted by $2\pi \sin(\Theta_E)d\Theta_E$ to approximate the integration over 2π solid angle. For diffuse wave transmission through random media, the escape function is analytically derived, and given by[63,66]

$$P(\omega; \mu_e) = \frac{3}{2}\mu_e[\tau_e(\omega) + \mu_i]\cdot[1 - R_D(\omega; \mu_i)] \quad (3)$$

Here, $\cos^{-1}(\mu_i)$ is the angle inside the sample, which will be related to $\cos^{-1}(\mu_e)$ using Snell's law.[67] $R_D(\omega; \mu_i)$ is the angle- and frequency-dependent internal-reflection coefficient. Finally, $\tau_e(\omega) = z_e(\omega)/l(\omega)$ is the extrapolation length ratio, defined by the extrapolation length $z_e(\omega)$ and the transport mean free path $l(\omega)$ of the sample, where $z_e(\omega)$ is the distance from the samples' surface at which the diffuse intensity extrapolates to 0. $\tau_e(\omega)$ can be expressed as a function of the angle-averaged reflectivity of the sample boundaries $\bar{R}_D(\omega)$,[62−64]

$$\tau_e(\omega) = \frac{2}{3}\left[\frac{1 + \bar{R}_D(\omega)}{1 - \bar{R}_D(\omega)}\right] \quad (4)$$

The average reflectivity $\bar{R}_D(\omega)$ depends on the angle- and frequency-dependent internal reflection coefficient $R_D(\omega; \mu_i)$ as[63,64,66]

$$\bar{R}_D(\omega) = \frac{3C_2(\omega) + 2C_1(\omega)}{3C_2(\omega) - 2C_1(\omega) + 2}, \quad \text{with} \quad (5)$$

$$C_n(\omega) = \int_0^1 R_D(\omega; \mu_i)\mu_i^n d\mu_i \quad (6)$$

Hence, the escape function from eq 3 can be evaluated if $R_D(\omega; \mu_i)$ is known. So far, the derivation of the model was general and derived for random photonic media in which light transport is diffuse due to multiple scattering. This isotropic model for $P(\omega; \mu_e)$ successfully described experimental results on random media when $R_D(\omega; \mu_i)$ was modeled using Fresnel's law in combination with an effective refractive index.[68] However, this neglects the stop bands typical of photonic crystals. Hence, a different approach is needed to find an expression for $R_D(\omega; \mu_i)$ and expand the escape-function model to describe photonic crystals as pioneered by our group.[65]

The reflectivity from titania inverse opals is mainly determined by simultaneous coupled Bragg diffraction from (111) and (200) planes.[56] The internal reflection coefficient is therefore modeled as the sum of two Gaussian reflection peaks,[21] that is,

$$R_D(\omega; \mu_i) = R_1(\mu_i)\exp\left\{-\frac{[\omega - \omega_1(\mu_i)]^2}{2\Delta\omega_1(\mu_i)^2}\right\} + R_2(\mu_i)\exp\left\{-\frac{[\omega - \omega_2(\mu_i)]^2}{2\Delta\omega_2(\mu_i)^2}\right\} \quad (7)$$

with angle-dependent peak reflectivities $R_{1,2}(\mu_i)$, widths $\Delta\omega_{1,2}(\mu_i)$, and center frequencies $\omega_{1,2}(\mu_i)$. (For these measurements, the parameters used at $\mu_i = 1$ are as follows: $R_1(1) = 0.7$; $R_2(1) = 0.3$; $\omega_1(1) = 0.797$; $\omega_2(1) = 1.33$; $\Delta\omega_1(1) = 0.064$; $\Delta\omega_2(1) = 0.071$.) These center frequencies cannot be described by simple Bragg diffraction by 111 and 200 planes, since the two diffraction conditions interact and show a large avoided crossing.[56] Therefore, band structure calculations are used to calculate $\omega_{1,2}(\mu_i)$.[65] For $R_{1,2}(\mu_i)$ and $\Delta\omega_{1,2}(\mu_i)$, normal incidence reflectivity data are used, and it is reasonably assumed that these four parameters are smooth functions of μ_i. This expanded escape-function model can now be directly compared with the results we measured on photonic crystals by evaluating the model as a function of both incidence angle and normalized frequency ω/ω_{111}, where normalization is relative to the calculated normal-incidence stop gap center frequency ω_{111}.

Comparison of Experiment with Escape-Function Model. Figure 6 shows the escape function $P(\omega; \Theta_E)$ over large frequency and angular ranges as derived from experiments and theory. Figure 6a is derived from three experiments on samples with different stop band frequencies ω_{111}. The results from the different experiments are separated by the horizontal, gray lines. At low frequencies ($\omega/\omega_{111} < 0.92$), the crystal is in the long-wavelength limit; hence, there is no stop band, and the emission escape probability decreases monotonously with Θ_E. The central part ($0.92 < \omega/\omega_{111} < 1.2$) shows a strong stop band in the escape probability due to the L-gap. As expected, the frequency of the stop band increases with the external angle. An enhanced escape probability is observed at $\omega/\omega_{111} \approx 1.05$ for the external angle $\Theta_E \approx 50°$. The enhancement of the escape probability stems from a redistribution of the light that is Bragg diffracted inside the photonic crystal, as discussed below. At high frequencies ($\omega/\omega_{111} > 1.15$), a region is observed with enhanced escape probability at small Θ_E. The escape probability rapidly decreases at larger angles. Dark areas at the largest frequencies point out the presence of inhibited escape probabilities caused by Bragg wave coupling from the (200) lattice planes.[56] For applications, we propose that this map (Figure 6) can be used to find the stop-band frequency ω_{111} that yields the desired angular-dependent escape probability at the frequency ω of choice.

Figure 6b shows the calculation from the expanded escape-function model. The calculated escape probability shows the same characteristics as the experimental results. There is a clear inhibition of escape probability starting at $\omega/\omega_{111} \approx 1.0$, for $\Theta_E = 0°$. The central frequency of this inhibition shows the same

dx.doi.org/10.1021/jp308590g | J. Phys. Chem. C 2013, 117, 3431−3439

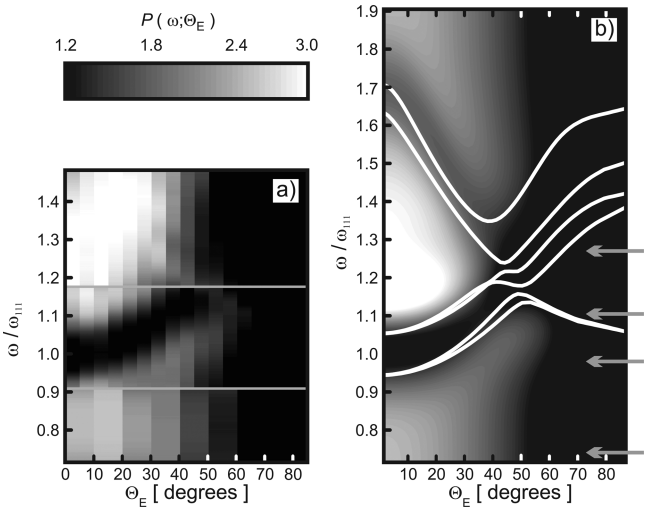

Figure 6. Escape probability $P(\omega; \Theta_E)$. (a) Experimental results from three data sets with different stop-band frequencies ω_{111}, separated by horizontal lines: ω_{111} = 5628 cm^{-1} (top); ω_{111} = 6945 cm^{-1} (middle); and ω_{111} = 9029 cm^{-1} (bottom) as determined from reflectivity measurements. The low-frequency region shows the expected Lambertian-like behavior. The central-frequency region shows clear inhibition of the escape probability due to the L-stop band. Regions of enhanced escape probability appear near ω/ω_{111} = 1.05 and 1.15 for $\Theta_E \approx 50°$ and 0°, respectively. (b) Result from the expanded escape-function model. The model is in very good agreement with the experimental results. The stop band caused by Bragg diffraction from (111) lattice planes is observed, together with the regions of enhanced escape probability. The higher order multiple Bragg wave diffraction is recognized by the inhibited escape-probability region that starts at ω/ω_{111} = 1.7 for Θ_E = 0° and continues to lower frequencies at larger angles. White curves show the lowest six bands along the LU direction, using parallel momentum ($k_\parallel$) conservation at the surface to transform internal propagation angles into external propagation angles.[56] The horizontal arrows indicate the frequencies of the cross sections used in Figure 7. The common gray scale range is limited for clarity.

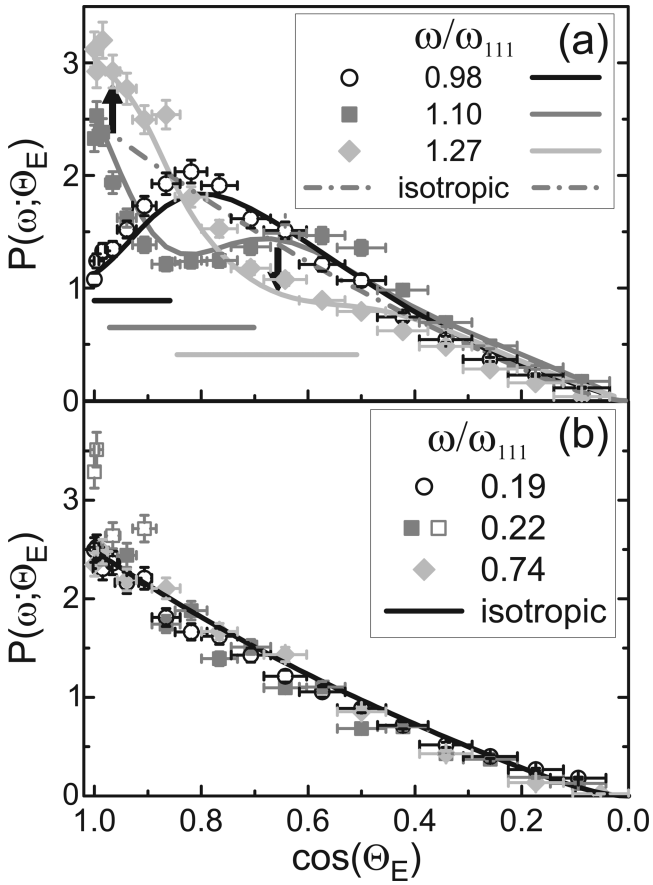

Figure 7. Cross sections of escape function at different reduced frequencies ω/ω_{111}. Symbols denote the measurements. (a) Results in the photonic range. Solid curves are results from the expanded escape-function model. Escape function versus cos Θ_E shows inhibition and enhancement of the escape probability with respect to the Lambertian distribution (dash-dotted line). Inside (outside) the stop bands the escape probability is inhibited (enhanced) up to 60% (34%) with respect to the Lambertian distribution. The frequency of the stop band is marked by the horizontal bars below the curves. The stop band moves to higher frequencies at larger angles. For the ω/ω_{111} = 1.27 case, the upward and downward pointing arrows, respectively, indicate the enhanced and inhibited escape probabilities with respect to the isotropic model. (b) Results in nonphotonic regime. Circles and squares are measured on the same sample with a stop band near ω_{111} = 33 600 cm^{-1}. The diamonds are data collected from a sample with ω_{111} = 9029 cm^{-1}. Only for ω/ω_{111} = 0.22, the experimental data deviate from the model (open squares), as a result of an emission intensity increase with time, during the experiment.

dependence on Θ_E as the experimental results. Another line of inhibited escape probability runs from ω/ω_{111} = 1.7 at Θ_E = 0° toward ω/ω_{111} = 1.2 at Θ_E = 50°. Multiple Bragg wave coupling causes the escape probability to be inhibited for angles larger than 40° and frequencies 1.10 < ω/ω_{111} < 1.35. This result agrees well with our experimental results. The regions with the measured, enhanced escape probability are also predicted by the model. Clearly, the expanded escape function very well describes the experimental data measured from these strongly photonic crystals. The white curves show the lowest 6 LU bands from a band structure calculation used to describe experiments in the visible regime.[65]

To compare the results from the model and the experiments in more detail, cross sections through the two-dimensional plots were made at the frequencies indicated by the arrows in Figure 6b. In contrast to Figure 6, the escape function is now plotted versus μ_e = cos Θ_E. In this representation, the escape function for isotropic emitters tends toward a line, simplifying comparison with experimental results. Figure 7a shows the escape function versus external angle at three different reduced frequencies in the photonic regime ($\omega/\omega_{111} \in \{0.98, 1.10, 1.27\}$). The dash-dotted line shows the regular escape-function model for isotropic (Lambertian) emitters. The stop band is clearly visible as the region where the escape probability is reduced with respect to the isotropic probability distribution. Outside the stop band, the escape probability is higher than the isotropic model such that the escape probability integrated over all angles is conserved. This probability enhancement is caused by a redistribution of the light inside the photonic crystal: for a certain angular range, the light Bragg diffracts back into the sample, where it becomes diffuse and escapes the sample at angles away from the Bragg condition. The enhancement is most profound close to the stop band. Further away from the stop band, the data converge to the isotropic case. The expanded escape-function model agrees very well with the experimental data. The experimental data appear even more explicit than the model predicts. Compared to Lambertian emission, inhibition of the emitted power as high as 60% is observed in the photonic crystal. Furthermore, the photonic crystal gives rise to emission power enhancements as high as 34%. For ω/ω_{111} = 0.98 and 1.10, the inhibition and

dx.doi.org/10.1021/jp308590g | J. Phys. Chem. C 2013, 117, 3431−3439

enhancement are observed over a cone with a top angle of $2\Theta_E = 60°$, which corresponds to a large solid angle of $2\pi(1 - \cos \Theta_E) = 0.84$ sr. The pronounced inhibition at $\omega/\omega_{111} = 1.10$, between $\cos \Theta_E = 0.97$ and 0.71, corresponds also to a large solid angle of 1.6 sr.

Figure 7b shows the escape function $P(\omega; \Theta_E)$ cross sections measured from two nonphotonic samples. Symbols denote measured data, and the line is calculated from the regular, isotropic model. There is no stop band. The data at $\omega/\omega_{111} = 0.19$ and 0.22 are measured from the same sample. The $\omega/\omega_{111} = 0.22$ data deviate from the model and show the sawtooth effect described in the Experimental Details section, which is caused by inhomogeneous spectral broadening at the blue side of the emission spectrum of the quantum dot ensemble. On the red side of the spectrum ($\omega/\omega_{111} = 0.19$), the data are in good agreement with the model. Clearly, the regular escape-function model fits the escape-function data from nonphotonic titania inverse opals very well over a very large range of reduced frequencies. Hence, we are able to model the escape function both from photonic and nonphotonic crystals, using our expression for the internal-reflection coefficient $R_D(\omega; \mu_i)$ (eq 7).

DISCUSSION

Photonic crystals have to date been divided into (1) optically thick samples where the thickness L is much larger than the transport mean free path l ($l/L \ll 1$) and (2) optically thin samples where the thickness is about the mean free path of light, or less ($l/L \gtrsim 1$).[31] Inside optically thick samples, light that is Bragg diffracted back into the sample scatters off defects and becomes diffuse. Subsequently, this light can exit the structure at angles completely uncorrelated with the original emission wave vector. This results in the redistribution of the emission intensity over escape angles. In emission measurements, this redistribution causes an emission intensity increase at the edges of the stop band that is clearly not related to effects in the LDOS; see also refs 65 and 69. In optically thin samples, most emitted light escapes the sample ballistically. There is only little scattering in these structures. However, Bragg diffraction may still decrease the emission intensity considerably in specific directions.[16,25]

The samples used in this study have $L/l \approx 3 - 9$, which means that, for the quantum dot emission, the sample is in the intermediate regime between optically thick ($l \ll L$) and optically thin ($l \gtrsim L$). As a consequence, a significant part of the light emitted by the dots is not very diffuse before escaping the photonic crystal. Still, our model that is based on diffusion theory describes the experiments very well. Although the validity of the diffuse transport equation of the emitted light may be questioned, it is believed that the model's requirement for a distributed light source is fulfilled as (1) the excitation of the quantum dots is diffuse because the sample is optically thick for the 532 nm excitation light ($L/l > 51$), (2) the absorption length of the excitation light is about two orders larger than the sample thickness, due to the low concentration of quantum dots and hence the excitation light distribution is diffuse, and (3) the emission of the quantum dots randomizes the wave vector $\vec{\mathbf{k}}$.

The good correspondence between the model and the experimental results demonstrate the applicability of the escape-function model to a new regime in photoluminesence experiments. This regime is illustrated in Figure 8 and defined by the ratio of the sample thickness L and the transport mean free paths of the emitted light (l_{em}) and the excitation light (l_{exc}), respectively. The escape function has been used successfully in the optically thick regime, with $L \gg l_{em}$, l_{exc}. The model is not suited for the optically thin samples, where $L \ll l_{em}$, l_{exc}. In this paper, a new *mixed regime* is added with $L \gg l_{exc}$ and $L \approx l_{em}$. As discussed above, the escape-funtion model, based on diffusion theory and expanded to photonic crystals, was successfully applied in this new regime.

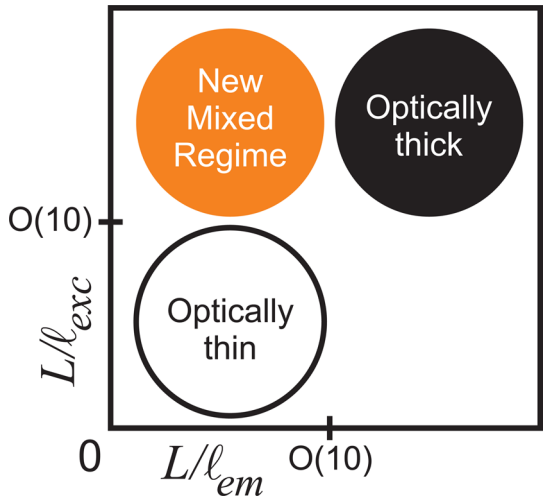

Figure 8. Schematic representation of different regimes in photoluminesence experiments. The regimes are defined by the transport mean free path of the emitted light l_{em} and the excitation light l_{exc}, with respect to the sample thickness L. The *optically thin* regime has been studied before in refs 16 and 25 whereas the *optically thick* regime was studied in refs 20, 21, and 69. A new *mixed regime* is defined where the excitation light is diffuse and the emitted light is on the edge of being diffuse or ballistic. The escape-function model based on diffusion theory is successfully applied in this new regime.

Strong photoluminescence modifications may easily lead to misinterpretation of experimental findings. There are various examples where an attenuation in a small frequency range of the photoluminescence emission spectrum are attributed to a change in the widely pursued local density of states of the emitter.[14,18,70−72] In contrast, the attenuation is caused by Bragg diffraction that causes a nonisotropic escape probability. This effect can be understood from eq 1: the emitters properties and the LDOS are contained in $I_{tot}(\omega)$, whereas the experimentalist measures $I(\omega; \mu_e)$. In photonic crystals, these spectra cannot be linked without considering the escape function $P(\omega; \mu_e)$. Without the escape function, it cannot be recognized if light is redistributed over directions that do not show Bragg diffraction.

CONCLUSIONS

We have studied the angular distribution of near-infrared spontaneous emission (1200−1550 nm) from PbSe quantum dots inside 3D titania inverse opals. We have observed angular redistribution of the light over the exit angle, caused by a combination of light diffusion and Bragg diffraction in the photonic crystals. The escape function was extracted from the experimental data and explained with a diffusion model, expanded to photonic crystals. We found a very good agreement between the measurement and the model. This is the first time for the model to be applied to the regime of diffuse excitation in combination with optically rather thin

dx.doi.org/10.1021/jp308590g | J. Phys. Chem. C 2013, 117, 3431−3439

samples for the emitted light. Furthermore, an interpretation of emission enhancement at the sides of the stop bands is given in terms of angular redistribution of emission intensities. In the photonic crystal, an escape inhibition of 60% is observed as well as an enhancement of 34%, both with respect to the escape distribution from nonphotonic samples. Typically the emission is enhanced or inhibited over solid angles larger than 0.84 sr.

AUTHOR INFORMATION

Corresponding Author

*E-mail: b.h.husken@alumnus.utwente.nl.

Notes

The authors declare no competing financial interest.

ACKNOWLEDGMENTS

Charles Uju and Steven Kettelarij are thanked for the fabrication of the titania inverse opals. This research was supported by NanoNed, a nanotechnology programme of the Dutch Ministry of Economic Affairs, by a grant from the "Stichting Technische Wetenschappen" (STW) to W.L.V., and by a VENI & VIDI fellowship by NWO to A.F.K. This work is also part of the research programme of the "Stichting voor Fundamenteel Onderzoek der Materie" (FOM), which is financially supported by the NWO.

REFERENCES

(1) Yablonovitch, E. *Phys. Rev. Lett.* **1987**, *58*, 2059−2062.
(2) Vahala, K. J. *Nature* **2003**, *424*, 839−846.
(3) Noda, S.; Fujita, M.; Asano, T. *Nat. Photonics* **2007**, *1*, 449−458.
(4) Sprik, R.; van Tiggelen, B. A.; Lagendijk, A. *Europhys. Lett.* **1996**, *35*, 265−270.
(5) Koenderink, A. F.; Bechger, L.; Schriemer, H. P.; Lagendijk, A.; Vos, W. L. *Phys. Rev. Lett.* **2002**, *88*, 143903.
(6) Ogawa, S.; Imada, M.; Yoshimoto, S.; Okano, M.; Noda, S. *Science* **2004**, *305*, 227−229.
(7) Lodahl, P.; van Driel, A. F.; Nikolaev, I. S.; Irman, A.; Overgaag, K.; Vanmaekelbergh, D.; Vos, W. L. *Nature* **2004**, *430*, 654−657.
(8) Fujita, M.; Takahashi, S.; Tanaka, Y.; Asano, T.; Noda, S. *Science* **2005**, *308*, 1296−1298.
(9) Nikolaev, I. S.; Lodahl, P.; van Driel, A. F.; Koenderink, A. F.; Vos, W. L. *Phys. Rev. B* **2007**, *75*, 115302.
(10) Vallée, R. A. L.; Baert, K.; Kolaric, B.; van der Auweraer, M.; Clays, K. *Phys. Rev. B* **2007**, *76*, 045113.
(11) Julsgaard, B.; Johansen, J.; Stobbe, S.; Stolberg-Rohr, T.; Sünner, T.; Kamp, M.; Forchel, A.; Lodahl, P. *Appl. Phys. Lett.* **2008**, *93*, 094102.
(12) Jorgensen, M. R.; Galusha, J. W.; Bartl, M. H. *Phys. Rev. Lett.* **2011**, *107*, 143902.
(13) Leistikow, M. D.; Mosk, A. P.; Yeganegi, E.; Huisman, S. R.; Lagendijk, A.; Vos, W. L. *Phys. Rev. Lett.* **2011**, *107*, 193903.
(14) Yamasaki, T.; Tsutsui, T. *Appl. Phys. Lett.* **1998**, *72*, 1957−1959.
(15) Petrov, E. P.; Bogomolov, V. N.; Kalosha, I. I.; Gaponenko, S. V. *Phys. Rev. Lett.* **1998**, *81*, 77−80.
(16) Megens, M.; Wijnhoven, J. E. G. J.; Lagendijk, A.; Vos, W. L. *J. Opt. Soc. Am. B* **1999**, *16*, 1403−1408.
(17) Schriemer, H. P.; van Driel, H. M.; Koenderink, A. F.; Vos, W. L. *Phys. Rev. A* **2001**, *63*, 011801.
(18) Lin, Y.; Zhang, J.; Sargent, E. H.; Kumacheva, E. *Appl. Phys. Lett.* **2002**, *81*, 3134−3136.
(19) de Dood, M. J.; Polman, A.; Fleming, J. G. *Phys. Rev. B* **2003**, *67*, 115106.
(20) Bechger, L.; Lodahl, P.; Vos, W. L. *J. Phys. Chem. B* **2005**, *109*, 9980−9988.
(21) Nikolaev, I. S.; Lodahl, P.; Vos, W. L. *Phys. Rev. A* **2005**, *71*, 053813.
(22) Barth, M.; Gruber, A.; Cichos, F. *Phys. Rev. B* **2005**, *72*, 085129.
(23) Li, M.; Zhang, P.; Li, J.; Zhou, J.; Sinitskii, A.; Abramova, V.; Klimonsky, S. O.; Tretyakov, Y. D. *Appl. Phys. B: Lasers Opt.* **2007**, *89*, 251−255.
(24) Noh, H.; Scharrer, M.; Anderson, M. A.; Chang, R. P. H.; Cao, H. *Phys. Rev. B* **2008**, *77*, 115136.
(25) Brzezinski, A.; Lee, J.-T.; Slinker, J. D.; Malliaras, G. G.; Braun, P. V.; Wiltzius, P. *Phys. Rev. B* **2008**, *77*, 233106.
(26) Koenderink, A. F.; Megens, M.; van Soest, G.; Vos, W. L.; Lagendijk, A. *Phys. Lett. A* **2000**, *268*, 104−111.
(27) Vlasov, Y. A.; Astratov, V. N.; Baryshev, A. V.; Kaplyanskii, A. A.; Karimov, O. Z.; Limonov, M. F. *Phys. Rev. E* **2000**, *61*, 5784−5793.
(28) Huang, J.; Eradat, N.; Raikh, M. E.; Vardeny, Z. V.; Zakhidov, A. A.; Baughman, R. H. *Phys. Rev. Lett.* **2001**, *86*, 4815−4818.
(29) Astratov, V. N.; Adawi, A. M.; Fricker, S.; Skolnick, M. S.; Whittaker, D. M.; Pusey, P. N. *Phys. Rev. B* **2002**, *66*, 165215.
(30) Koenderink, A. F.; Lagendijk, A.; Vos, W. L. *Phys. Rev. B* **2005**, *72*, 153102.
(31) Koenderink, A. F.; Vos, W. L. *J. Opt. Soc. Am. B* **2005**, *22*, 1075−1084.
(32) Kaas, B. C.; van Tiggelen, B. A.; Lagendijk, A. *Phys. Rev. Lett.* **2008**, *100*, 123902.
(33) Koenderink, A. F. *Emission and Transport of Light in Photonic Crystals*. Ph.D. Thesis, University of Twente, Enschede, The Netherlands, 2003.
(34) Muskens, O. L.; Koenderink, A. F.; Vos, W. L. *Phys. Rev. B* **2011**, *83*, 155101.
(35) García, P. D.; Sapienca, R.; Toninelli, C.; López, C.; Wiersma, D. S. *Phys. Rev. A* **2011**, *84*, 023813.
(36) Blanco, A.; Chomski, E.; Grabtchak, S.; Ibisate, M.; John, S.; Leonard, S. W.; Lopez, C.; Meseguer, F.; Miguez, H.; Mondia, J. P.; Ozin, G. A.; Toader, O.; van Driel, H. M. *Nature* **2000**, *405*, 437−440.
(37) Vlasov, Y. A.; Bo, X. Z.; Sturm, J. C.; Norris, D. J. *Nature* **2001**, *414*, 289−293.
(38) Woldering, L. A.; Tjerkstra, R. W.; Jansen, H. V.; Setija, I. D.; Vos, W. L. *Nanotechnology* **2008**, *19* (145304), 1−11.
(39) Wise, F. W. *Acc. Chem. Res.* **2000**, *33*, 773−780.
(40) Du, H.; Chen, C.; Krishnan, R.; Krauss, T. D.; Harbold, J. M.; Wise, F. W.; Thomas, M. G.; Silcox, J. *Nano Lett.* **2002**, *2*, 1321−1324.
(41) Wehrenberg, B. L.; Wang, C.; Guyot-Sionnest, P. *J. Phys. Chem. B* **2002**, *106*, 10634−10640.
(42) Moreels, I.; Lambert, K.; De Muynck, D.; Vanhaecke, F.; Poelman, D.; Martins, J. C.; Allan, G.; Hens, Z. *Chem. Mater.* **2007**, *19*, 6101−6106.
(43) Li, J.; Jia, B.; Zhou, G.; Bullen, C.; Serbin, J.; Gu, M. *Adv. Mater.* **2007**, *19*, 3276−3280.
(44) Li, J.; Jia, B.; Zhou, G.; Gu, M. *Appl. Phys. Lett.* **2007**, *91*, 254101.
(45) Schaller, R. D.; Klimov, V. I. *Phys. Rev. Lett.* **2004**, *92*, 186601.
(46) Trinh, M. T.; Houtepen, A. J.; Schins, J. M.; Hanrath, T.; Piris, J.; Knulst, W.; Goossens, A. P. L. M.; Siebbeles, L. D. A. *Nano Lett.* **2008**, *8*, 1713−1718.
(47) Neale, N. R.; Lee, B. G.; Kang, S. H.; Frank, A. J. *J. Phys. Chem. C* **2011**, *115*, 14341−14346.
(48) Harbold, J. M.; Du, H.; Krauss, T. D.; Cho, K.-S.; Murray, C. B.; Wise, F. W. *Phys. Rev. B* **2005**, *72*, 195312.
(49) Lifshitz, E.; Brumer, M.; Kigel, A.; Sashchiuk, A.; Bashouti, M.; Sirota, M.; Galun, E.; Burshtein, Z.; Le Quang, A. Q.; Ledoux-Rak, I.; Zyss, J. *J. Phys. Chem. B* **2006**, *110*, 25356−25365.
(50) Li, J.; Jia, B.; Zhou, G.; Gu, M. *Opt. Express* **2006**, *14*, 10740−10745.
(51) Wijnhoven, J. E. G. J.; Vos, W. L. *Science* **1998**, *281*, 802−804.
(52) Wijnhoven, J. E. G. J.; Bechger, L.; Vos, W. L. *Chem. Mater.* **2001**, *13*, 4486−4494.
(53) Koenderink, A. F.; Bechger, L.; Lagendijk, A.; Vos, W. L. *Phys. Status Solidi A* **2003**, *197*, 641−661.
(54) Husken, B. H.; Woldering, L. A.; Blum, C.; Vos, W. L. *J. Microsc.* **2009**, *233*, 18−23.
(55) Lakowicz, J. R. *Principles of Fluorescence Spectroscopy*, 2nd ed.; Kluwer Academic/Plenum Publishers: New York, 1999.

(56) van Driel, H. M.; Vos, W. L. *Phys. Rev. B* **2000**, *62*, 9872−9875.
(57) Galisteo-Lopez, J.-F.; Vos, W. L. *Phys. Rev. E* **2002**, *66*, 036616.
(58) Kop, R. H. J.; de Vries, P.; Sprik, R.; Lagendijk, A. *Phys. Rev. Lett.* **1997**, *79*, 4369−4372.
(59) Ishimaru, A. *Appl. Opt.* **1978**, *17*, 348−352.
(60) van Albada, M. P.; Lagendijk, A. *Phys. Rev. Lett.* **1985**, *55*, 2692−2695.
(61) Sheng, P. *Scattering and Localization of Classical Waves in Random Media*; World Scientific: Singapore, 1990.
(62) Lagendijk, A.; Vreeker, R.; de Vries, P. *Phys. Lett. A* **1989**, *136*, 81−88.
(63) Zhu, J. X.; Pine, D. J.; Weitz, D. A. *Phys. Rev. A* **1991**, *44*, 3948−3959.
(64) Vera, M. U.; Durian, D. J. *Phys. Rev. E* **1996**, *53*, 3215−3224.
(65) Koenderink, A. F.; Vos, W. L. *Phys. Rev. Lett.* **2003**, *91*, 213902-1−213902-4.
(66) Durian, D. J. *Phys. Rev. E* **1994**, *50*, 857−866.
(67) Born, M.; Wolf, E. *Principles of Optics*, 4th ed.; Cambridge University Press: Cambridge, U.K., 1997.
(68) Gómez Rivas, J.; Dau, D. H.; Imhof, A.; Sprik, R.; Bret, B. P. J.; Johnson, P. M.; Hijmans, T. W.; Lagendijk, A. *Opt. Commun.* **2003**, *220*, 17−21.
(69) Blum, C.; Mosk, A. P.; Nikolaev, I. S.; Subramaniam, V.; Vos, W. L. *Small* **2008**, *4*, 492−496.
(70) Blanco, A.; López, C.; Mayoral, R.; Míguez, H.; Meseguer, F.; Mifsud, A.; Herrero, J. *Appl. Phys. Lett.* **1998**, *73*, 1781.
(71) Yoshino, K.; Lee, S. B.; Tatsuhara, S.; Kawagishi, Y.; Ozaki, M.; Zakhidov, A. A. *Appl. Phys. Lett.* **1998**, *73*, 3506−3508.
(72) Romanov, S. G.; Fokin, A. V.; de La Rue, R. M. *Appl. Phys. Lett.* **2000**, *76*, 1656.